Adiabatic Capture Theory Applied to N + NH → N_2 + H at Low Temperature

Terry J. Frankcombe* and Gunnar Nyman†

Physical Chemistry, Department of Chemistry, Göteborg University, SE-412 96 Göteborg, Sweden

Received: August 9, 2007; In Final Form: October 11, 2007

The adiabatic capture centrifugal sudden approximation (ACCSA) has been applied to the ground state reaction N + NH → N_2 + H over the temperature range 2−300 K using an existent potential energy surface. The resultant thermal rate constants are in agreement with available rate constants from quasi-classical trajectory calculations but are significantly larger than the available experimentally derived rate. The calculated rate constants monotonically increase with increasing temperature but could only be approximately described with a simple Arrhenius-like form. Subtle quantum effects are evident in the initial rotational state resolved cross sections and rate constants.

1. Introduction

The NH radical is an important species in astrochemistry and combustion chemistry alike. In combustion the NH species is involved in NO_x formation in flames under fuel-rich conditions[1] and with nitrogen-containing fuels.[2] In astrochemical contexts, the NH radical is believed to be one of the most abundant nitrogen-containing species (after N and N_2) in both photodominated regions[3] and dark clouds.[4] This means reactions involving the NH radical are likely to have a strong influence on models of both combustion and astrochemistry.

In astrochemical contexts, the reaction

$$N + NH \rightarrow N_2 + H \qquad (1)$$

is of particular interest as it is a member of the small set of reactions among the likely network of reactions[3] that lead to the formation of N_2. While molecular nitrogen is not easily observed in interstellar space, the detections that have been made do not agree with current astrochemical models.[5,6]

There has been little study of reaction 1 at the low temperatures relevant to interstellar chemistry. This is exemplified by the fact that the widely used RATE 06 astrochemical reaction rate database[4] lists a single estimated temperature-independent rate constant, claimed to be applicable over the range 10−1400 K. The only experimental measurement reported is that of Hack et al.[7] This single measurement at 298 K gives a rate constant almost exactly half the 10−1400 K rate constant cited by RATE 06.

The reaction has been studied theoretically by Varandas and co-workers.[8−10] They proposed[8] and then refined[10] a global potential energy surface for the N_2H system based on high quality (MRCI/aug-cc-pVQZ) ab initio calculations. This surface has been used as the basis of a quasi-classical trajectory (QCT) and capture theory study[10] of reaction 1. The QCT reaction rates were calculated down to temperatures of 100 K. The restricted form of capture theory used did not yield results in agreement with the more extensive QCT calculations.

Despite the disagreement between previous capture theory and QCT calculations, reaction 1 is a good candidate for studying with a capture theory. Along the minimum energy path the reaction proceeds to a strongly bound collision complex (N_2H) without a potential barrier. A very small barrier exists on the exit channel from N_2H to the N_2 + H products, well below the energy of the entrance channel. The overall reaction is exothermic by 611 kJ/mol (6.33 eV), implying a very strong tendency for any N_2H formed to go on to produce the N_2 + H products. In this work we apply the adiabatic capture, centrifugal sudden approximation (ACCSA)[11,12] to reaction 1 to calculate capture (and hence reaction) cross sections and rate constants at the low temperatures relevant to astrochemical modeling.

2. Theory

The ACCSA model has been described in detail in the literature[11−14] and so shall be described only briefly here.

Working throughout in atomic units (so that $\hbar = 1$), the Hamiltonian for atom−rigid rotor collisions can be written as

$$\hat{H} = -\frac{1}{2\mu R}\frac{\partial^2}{\partial R^2}R + B\hat{\mathbf{j}}^2 + \frac{|\hat{\mathbf{J}} - \hat{\mathbf{j}}|^2}{2\mu R^2} + V(R,\theta) \qquad (2)$$

where R is the separation between the colliding atom and the center of mass of the rigid rotor, μ is the atom−rigid rotor reduced mass, B is the rotational constant of the rigid rotor, $\hat{\mathbf{j}}$ is the operator for the angular momentum of the rigid rotor, $\hat{\mathbf{J}}$ is the total angular momentum operator and $V(R,\theta)$ is the interaction potential with the angle θ specifying the orientation of the rigid rotor with respect to the atom. Applying the centrifugal sudden approximation (CSA), $|\hat{\mathbf{J}} - \hat{\mathbf{j}}|^2$ is replaced by the diagonal term $J(J+1) + \hat{\mathbf{j}}^2 - 2\Omega^2$, where Ω is the projection of the total angular momentum on the atom−rigid rotor center of mass vector in the asymptotic region. Such an approximation uncouples states of different Ω. Thus for $J = 0$, at a series of discrete values of R and for $|\Omega| \leq j$ the Hamiltonian can be expanded in terms of spherical harmonics and diagonalized to yield a set of rotationally adiabatic potential energy curves $\epsilon_{j,\Omega}(R)$.

For any J, j, and Ω, the adiabatic capture approximation assigns unit reaction probability if the initial collision energy E_c lies above the maximum of the effective potential given by

* Corresponding author. E-mail: terry@chem.gu.se, t.frankcombe@chem.leidenuniv.nl.

† E-mail: nyman@chem.gu.se.

10.1021/jp076422d CCC: $37.00
Published on Web 11/29/2007

$$V_j^{J,\Omega}(R) = \epsilon_{j,\Omega}(R) + \frac{J(J+1)}{2\mu R^2} - Bj(j+1) \qquad (3)$$

for separations R lying in the region outside the "captured" state (from where reaction to products is assumed to be inevitable), and zero otherwise. With this approximation the partial wave summation for the total reaction cross section as a function of initial j and collision energy E_c can be expressed as[13]

$$\sigma_j(E_c) = \frac{\pi}{2\mu E_c(2j+1)}\left\{\sum_{\Omega=-j}^{j}[J_{max}(j,\Omega,E_c)+1]^2 - \frac{j(j+1)(2j+1)}{3}\right\} \qquad (4)$$

where $J_{max}(j,\Omega,E_c)$ is the highest J at which the capture reaction can occur. [More precisely, $J_{max}(j, \Omega, E_c)$ is the smallest J for which $\max_R\{V_j^{J+1,\Omega}(R)\} > E_c$ for R outside the capture region. Thus when no reaction is possible, even at $J = 0$, $J_{max} = -1$, contributing nothing to the sum in eq 4.] Equation 4 relies on the relation

$$\sum_{\Omega=-\min(J,j)}^{\min(J,j)}\Omega^2 = 2\sum_{\Omega=1}^{\min(J,j)}\Omega^2 \approx 2\sum_{\Omega=1}^{j}\Omega^2 = \frac{j(j+1)(2j+1)}{3} \qquad (5)$$

which is a *numerical* approximation for the partial wave summation terms in which $J < j$. This approximation is justified by noting that usually J_{max} is much larger than j so that $J \geq j$ terms dominate σ_j. Note that in the absence of this approximation ACCSA is formally identical[13] to the statistical adiabatic channel model (SACM).[15]

From σ_j initial rotational state resolved thermal reaction rates at temperature T are given by

$$k_j(T) = \left[\frac{8}{\pi\mu(k_B T)^3}\right]^{1/2}\int_0^\infty E_c\sigma_j(E_c)\exp\left(\frac{-E_c}{k_B T}\right)dE_c \qquad (6)$$

where k_B is the Boltzmann constant. Finally, total thermal rate constants $k(T)$ can be obtained from $k_j(T)$ by a Boltzmann average over initial rotational states j.

3. Computational Details

The adiabatic potential energy curves $\epsilon_{j,\Omega}(R)$ resulting from the diagonalization of the CSA Hamiltonian depend on the potential matrix elements

$$\int Y_j^{\Omega *}(\theta,0)\, V(R,\theta)\, Y_{j'}^{\Omega}(\theta,0)\, d\tau \qquad (7)$$

where Y_j^{Ω} are the spherical harmonics used as a rotational basis set. The usual way to evaluate these matrix elements when applying the ACCSA is to first decompose the potential into a sum of Legendre polynomials. The matrix elements in (7) of the fitted potentially can then be expressed analytically as a sum of Wigner 3j symbols. In this work we do not employ such an approach. Instead, we evaluate eq 7 numerically using an adaptive integration routine.[16] Although numerical experiments have indicated that a relative error tolerance for the evaluation of the integrals in (7) as large as 10^{-5} do not effect the results, for the calculations reported here parameters were chosen to converge the matrix elements to a relative error of 10^{-9}.

In the current work special care has been taken to evaluate $J_{max}(j,\Omega,E_c)$ accurately. Maxima in $V_j^{J,\Omega}(R)$ were identified from an initial grid of 150 points in R. For each considered E_c, the potentials were evaluated at additional points around these maxima in an adaptive manner until $J_{max}(j,\Omega,E_c)$ could be identified definitively using pessimistic finite difference criteria. This approach was more reliable and required less computational effort than naively increasing the R grid density everywhere.

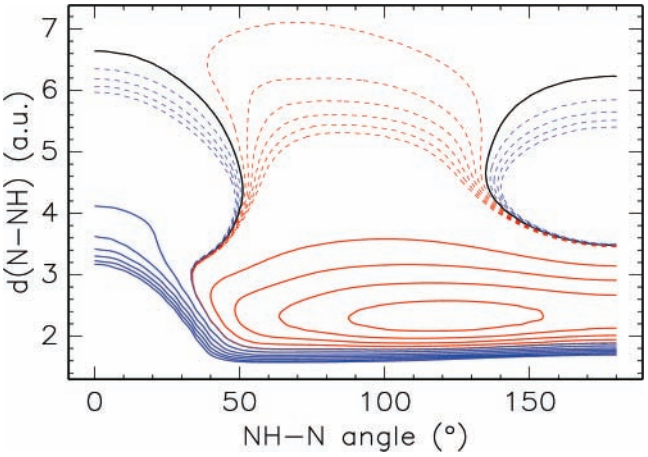

Figure 1. Potential for N + NH with the NH fragment frozen at the internuclear separation of 1.965 a_0, as a function of the angle between the fragment centers of mass axis and the NH fragment axis (with 180° being linear NHN), and the NH−N center of mass separation. Solid contours spaced at intervals of 0.05 E_h from the lowest at −0.2 E_h. Positive, negative, and zero contours shown in blue, red and black, respectively. Additional contours separated by 0.0005 E_h shown either side of the zero energy contour.

Evaluating the integral in eq 6 requires some consideration, as the discrete nature of $J_{max}(j,\Omega,E_c)$ (an integer function of the continuous variable E_c) means σ_j, and thus the integrand of eq 6, exhibits a large number of discontinuities. These integrand discontinuities make evaluation of the integral with the adaptive integrators used for the potential matrix elements problematic. Additionally, the integrand is strongly peaked at low temperatures. Previous implementations of ACCSA have fit σ_j to a power law that allows eq 6 to be integrated analytically. An alternate, exact scheme is possible, in which the set of energies E_c at which $J_{max}(j,\Omega,E_c)$ increases are identified for each j and Ω. The integral in eq 6 can then be evaluated analytically on each interval between J_{max} jump energies.

Rather than the above approaches, in the present work it was found that a simple Riemann sum evaluation of eq 6 provided easily controllable accuracy and reliable convergence. The integration range was set dynamically in such a way that the integrand at the upper limit of the integration range was at least 6 orders of magnitude smaller than the maximum value of the integrand. The integrals were well converged when using 1000 terms in the Riemann sum.

In this work all valid j and Ω were included up to a cutoff $\mathscr{J}$. That is, $\epsilon_{j,\Omega}$ were considered for all $|\Omega| \leq j$, $0 \leq j \leq \mathscr{J}$. The computational effort scales with $\mathscr{J}^3$. The calculated rate constants were found to be well converged for $\mathscr{J} = 15$.

The N + NH interaction was described using the double many-body expansion (DMBE) potential of Caridade et al.[10] This potential is a modification of the previous DMBE potential,[8] with a refined three-body term to give a more accurate description of the long-range behavior in the N + NH entrance channel. The NH diatomic bond length was fixed at 1.965 a_0, yielding a rotational constant B of 7.555×10^{-5} E_h, corresponding to 16.58 cm^{-1}. The slice of the potential used in this work is shown in Figure 1. The barrierless minimum energy pathway for N atom approach to NH on this surface involves a

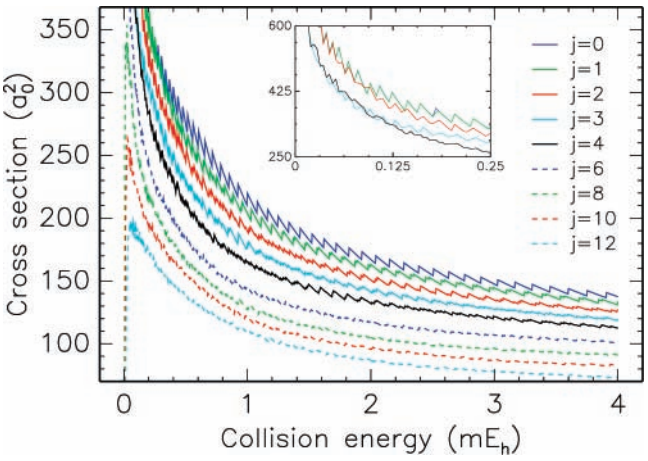

Figure 2. Selected calculated capture cross sections for a range of initial j, as a function of collision energy. The inset shows detail at low collision energy for $j \leq 4$.

moderate amount of relative rotation of the NH fragment but remains approximately T-shaped. At the most restricted point (in the vicinity of 4.5 a_0 separation) almost half of the angular range presents no potential barrier to association. Note that the single sheet N_2H potential energy surface is a doublet surface with the N + NH entrance channel corresponding to the N and NH fragments in their electronic ground states (^4S and $^3\Sigma^-$, respectively).

4. Results

The calculated initial rotational state resolved capture cross sections are shown in Figure 2. The larger of the discontinuities mentioned in section 3 are clearly visible in this plot. As a function of energy, the cross sections calculated by eq 4 were quite rough; many discontinuities are too small to be resolved on the scale of Figure 2. That J_{max} undergoes a regular sequence of integral jumps as E_c increases, with different spacing for different Ω, combined with the restriction that $|\Omega| \leq j$, yielded $j + 1$ identifiable overlapped sequences of jumps in σ_j. Thus, although the calculated cross sections look smoother for higher j, the number and frequency of discontinuities increased with j. In the absence of the capture approximation it is likely that these discontinuities would be smoothed by tunneling and other non-unit reaction probability effects. Thus it is unclear whether such quantum effects would be experimentally observable.

The cross sections generally decreased with increasing initial collision energy. This was because the centrifugal barriers relevant for low collisional energies were reduced by the attractive region of the N + NH potential. Thus at low collisional energies J_{max} was larger than one would expect from just the rotational terms of eq 3. This means that the E_c^{-1} behavior of the first term in eq 4—introduced by the $R \rightarrow \infty$ boundary conditions[17]—dominated until high enough energies were reached for the $J_{max} \propto E_c^{1/2}$ implied by the J term of eq 3 to yield cross sections tending to energy independence [canceling the E_c^{-1} prefactor in eq 4 with the dominant J_{max}^2 term].

The N + NH potential also had a strong effect on the j-dependence of the capture cross sections. The adiabatic potential energy curves $\epsilon_{j,\Omega}$ include rotationally averaged contributions from the potential through the potential matrix elements, (7). At high j the calculated $\epsilon_{j,\Omega}$ at small separations were increased by rotationally averaged contributions from the repulsive regions of the potential (cf. Figure 1), particularly for small Ω. Thus the capture region of the adiabatic potentials became inaccessible in this regime. Physically, this can be visualized as the incoming N atom being knocked away by interactions with the atoms of the diatomic (particularly the H atom end) before it could enter the potential well of the T-shaped geometry. At relatively high j the capture well disappeared completely from the calculated effective potentials $V_j^{J,\Omega}$ for low Ω. It should be noted that both the rotationally adiabatic capture and centrifugal sudden approximations are likely to perform poorly in these regimes. The presence of a repulsive barrier on the potential for collinear NH···N added to the complexity of the j dependence, with multiple maxima observed on the calculated effective potentials for some regions of (J,Ω,j) space. In all cases the capture approximation was applied according to the highest barrier in $V_j^{J,\Omega}$ at separations greater than those for the capture well in $V_j^{J,\Omega}$. Where there was no capture well the reaction probability was taken as zero for all energies.

The effect of the rotationally averaged repulsive regions of the intermolecular potential on the adiabatic potentials $\epsilon_{j,\Omega}$ was evident in the calculated cross sections in a number of ways. At most collision energies the calculated cross sections depended quite strongly on j. At higher j and low collision energies, the rotationally averaged potential barriers dominated over the attractive part of the potential leading to the drops in the cross sections seen in Figure 2 for very low collision energies. For small values of j there were jumps in the calculated cross sections at low collision energy as j increased. This is highlighted in the inset of Figure 2, showing the calculated cross sections for $j \leq 4$ at low energies. Clearly for low energies σ_0, σ_1, and σ_2 tended to similar values, as did σ_3 and σ_4, but σ_3 and σ_4 were well separated from the $j < 3$ group.

These jumps as a function of j at constant E_c could be traced to the effect of repulsive regions of the intermolecular potential and the integral nature of the asymptotic initial state quantum numbers. For low collision energies the relevant centrifugal barriers occurred at large separation where the potential was weak, giving J_{max} a weak dependence on Ω and j [for which eq 2 implies cross sections nearly independent of j]. For low but nonzero j a barrier in the rotationally adiabatic potential associated with the collinear approach barriers in the N + NH potential (around $R = 5\ a_0$) caused zero reaction probabilities for small Ω channels. For $j = 3$, 4 the $\Omega = 0$ capture channel was inactive, removing a significant contribution to the capture cross sections, giving a jump in the calculated cross sections. For $j = 5$, 6 the $\Omega = \pm 1$ channels were also inactive due to the larger effect of the rotationally averaged barriers overcoming the weak attraction, giving another jump in the cross sections. At higher j a similar trend continued with Ω channels switching off. Such a quantum effect should in principle be observable in experimentally determined initial state resolved reaction cross sections.

The calculated initial diatomic rotational state selected rate constants are shown in Figure 3. All the features highlighted above for the capture cross sections are evident in the resultant rate constants. Generally the rate constants decreased with increasing j. The clustering of cross sections for different j as the collision energy was reduced (due to the switching off of Ω channels) was reflected in the corresponding groups of state selected rate constants ($j = 0$, 1, 2, $j = 3$, 4, $j = 5$, 6 etc.) tending to the same values as the temperature was reduced. At very low temperatures these rates diverged again as the longer-range potential barriers prevented capture at very low collision energies (the drops in the higher j cross sections at low energy in Figure 2, most visible in k_3 and k_4 of those rate constants shown in Figure 3).

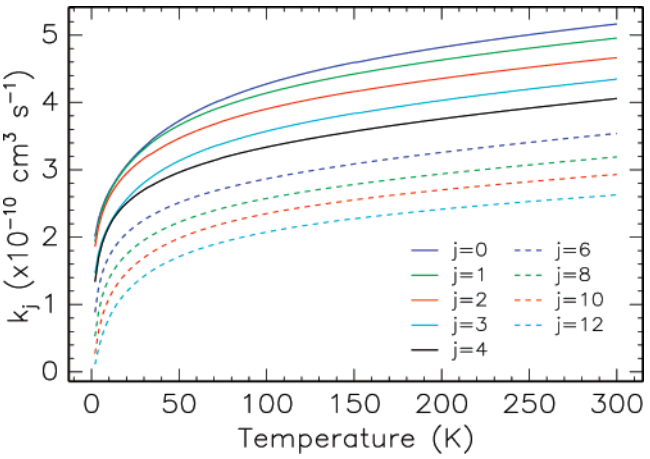

Figure 3. Selected calculated initial rotational state resolved rate constants.

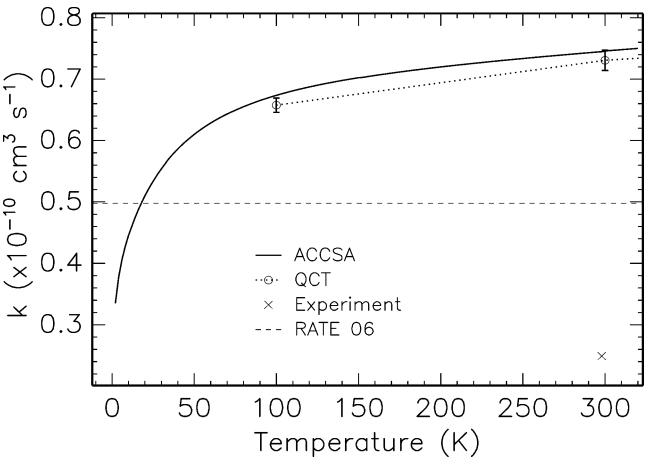

Figure 4. Thermal N + NH reaction rate constants. ACCSA results from this work, QCT results from Caridade et al.,[10] the experimental measurement of Hack et al.[7] and the temperature-independent value from the RATE 06 database.[4]

The calculated thermal capture rate constants are shown in Figure 4. Note that the rates shown and discussed below are the Boltzmann average of the $k_j(T)$ rates, multiplied by a factor of $^1/_6$. This factor comes from dividing the spin multiplicity of the N + NH potential energy surface (a doublet surface) by those for the reactants (quartet for N and triplet for NH). The rate constants decrease monotonically as the temperature is reduced below 300 K. Caridade et al.[10] performed QCT simulations of the N + NH reaction on the potential energy surface used in this work, mostly at higher temperatures. The QCT-derived rate constants at relevant temperatures are shown in Figure 4 for comparison with the ACCSA results. The agreement is very good, with the ACCSA rates being slightly larger than the QCT rates, by an amount comparable to the uncertainty quoted for the QCT rates. This suggests that—at least at the temperates at which the QCT calculations were performed—nonadiabatic and recrossing effects are small and ACCSA is a good approximation.

These results are significantly different to the capture theory results published by Caridade et al.[10] We attribute this difference to the approximation used in that work, expressing the spherically averaged, rotationally adiabatic potential as a single inverse power term rather than the explicitly evaluated quantity of this work. That approximation [akin to asserting $\epsilon_{j,\Omega}(R) \propto R^{-n_{j,\Omega}}$] is particularly poor on the N + NH surface.

The only experimental measurement of the rate of the N + NH reaction was reported by Hack et al.[7] This 298 K value, also indicated in Figure 4, is smaller than the ACCSA and QCT rates at that temperature by a factor larger than 2.6. Further experimental measurements must be performed to confirm this discrepancy. (Note that the claim by Zhan et al.[18] that a rate constant equal to that of the N + NH_2 reaction was given by Whyte and Phillips[19] seems to be a misunderstanding of the latter report.)

TABLE 1: Polynomial Coefficients α_i and β_i for Fits to Calculated Thermal Rate Constants (K^{-i})

i	α_i	β_i
−2	17.531	7.8888×10^{-11}
−1	−0.74761	-6.6328×10^{-11}
0	1.0000	4.6629×10^{-11}
1	2.4084×10^{-3}	4.4034×10^{-13}
2	-9.6773×10^{-6}	-3.2208×10^{-15}
3	1.4448×10^{-8}	1.1153×10^{-17}
4		-1.4297×10^{-20}

The calculated rate constants were fit to an Arrhenius expression [$A \exp(-\gamma/T)$] by minimizing the mean squared error in the temperate range 2−300 K. The resulting fit ($A = 7.23 \times 10^{-11}$ cm^3 s^{-1}, $\gamma = 4.99$ K) was very poor, with the parameters given here for completeness only. The fit to the modified Arrhenius form

$$k(T) = A\tilde{T}^m \exp(-\gamma/T) \tag{8}$$

with $\tilde{T} = T/1$ K, $A = 3.91 \times 10^{-11}$ cm^3 s^{-1}, $m = 0.116$, and $\gamma = 0.792$ K was better but still deviated from the calculated rates in most regions, by around 6% in the worst case (in the vicinity of 10 K) and generally by less than 2%. An expression with a polynomial dependence on temperature in the preexpontial factor:

$$k(T) = A\left(\sum_{i=-2}^{3} \alpha_i T^i\right) \exp\left(\frac{-\gamma}{T}\right) \tag{9}$$

with $A = 6.1087 \times 10^{-11}$ cm^3 s^{-1}, $\gamma = 4.4685$ K and the polynomial coefficients α_i given in Table 1 provided a close fit to the calculated ACCSA rate constants. A purely polynomial fit

$$k(T) = \sum_{i=-2}^{4} \beta_i T^i \tag{10}$$

with the β_i of Table 1 gave a fit of similar quality to eq 9 in the 2−300 K range.

5. Conclusion

The rate constants calculated for the title reaction are shown in Figure 4. Fits to the calculated rates in the 2−300 K range are given by eqs 9 and 10 with the parameters given in the text and in Table 1. A lower quality fit to the modified Arrhenius form of eq 8 had $A = 3.91 \times 10^{-11}$ cm^3 s^{-1}, $m = 0.116$, and $\gamma = 0.792$ K. The calculated rate constant at 10 K was 4.45×10^{-11} cm^3 s^{-1}.

There is clear disagreement between the rates calculated in this work and the single existent experimental measurement of the rate constant. The agreement between the QCT and ACCSA calculations indicate that the calculated rate constants represent the true rate constants on the DMBE II potential energy surface, itself derived from high quality ab initio data. Clearly, more experimental measurements must be performed to shed further light on the discrepancy.

The ACCSA calculations performed in this work have revealed clear quantum effects in the initial rotational state resolved reaction cross sections and rates. At very low collision energies these quantities exhibited jumps and nonmonotonicities as a function of the initial rotational state j. Such an effect, dependent on the rotational constant B of the diatomic collision partner, should in principle be experimentally observable.

Acknowledgment. We thank Antonio Varandas for providing the source code for the potential of ref 10. We also thank David Edvardsson and Stefan Andersson for useful discussions. This work was supported by the Swedish Research Council and by the European Community's Human Potential Programme under contract MCRTN 512302, Molecular Universe.

References and Notes

(1) Hayhurst, A. N.; Hutchinson, E. M. *Combust. Flame* **1998**, *114*, 274.
(2) Williams, B. A.; Fleming, J. W. *Combust. Flame* **1997**, *110*, 1.
(3) Sternberg, A.; Dalgarno, A. *Astrophys. J. Suppl. Ser.* **1995**, *99*, 565.
(4) Woodall, J.; Agúndez, M.; Markwick-Kemper, A. J.; Millar, T. J. *Astron. Astrophys.* **2007**, *466*, 1197.
(5) Knauth, D. C.; Andersson, B. G.; McCandliss, S. R.; Moos, H. W. *Nature* **2004**, *429*, 636.
(6) Maret, S.; Bergin, E. A.; Lada, C. J. *Nature* **2006**, *442*, 425.
(7) Hack, W.; Gg. Wagner, H.; Zasypkin, A. *Ber. Bunsen-Ges. Phys. Chem.* **1994**, *98*, 156.
(8) Poveda, L. A.; Varandas, A. J. C. *J. Phys. Chem. A* **2003**, *107*, 7923.
(9) Caridade, P. J. S. B.; Rodrigues, S. P.; Sousa, J. F.; Varandas, A. J. C. *J. Phys. Chem. A* **2005**, *109*, 2356.
(10) Caridade, P. J. S. B.; Poveda, L. A.; Rodrigues, S. P. J.; Varandas, A. J. C. *J. Phys. Chem. A* **2007**, *111*, 1172.
(11) Clary, D. C. *Mol. Phys.* **1985**, *54*, 605.
(12) Dateo, C. E.; Clary, D. C. *J. Chem. Phys.* **1989**, *90*, 7216.
(13) Ramillon, M.; McCarroll, R. *J. Chem. Phys.* **1994**, *101*, 8697.
(14) Edvardsson, D.; Williams, C. F.; Clary, D. C. *Chem. Phys. Lett.* **2006**, *431*, 261.
(15) Troe, J. *J. Chem. Phys.* **1987**, *87*, 2773.
(16) de Doncker, E. *SIGNUM Newsletter* **1978**, *13*, 2−12.
(17) Pack, R. T. *J. Chem. Phys.* **1974**, *60*, 633.
(18) Zhan, J.; Huang, R.; Zhuang, Q.; Zhang, C. *Chem. Phys. Lett.* **1990**, *174*, 568.
(19) Whyte, A. R.; Phillips, L. F. *Chem. Phys. Lett.* **1983**, *102*, 451.